

## EVOLUTION OF SECONDARY FLOWS IN A TURBULENT BOUNDARY LAYER PAST A STEP-CHANGE IN WALL TOPOGRAPHY

**Takfarinas Medjnoun**

Aerodynamics and Flight Mechanics  
University of Southampton  
Southampton SO17 1BJ, UK  
t.medjnoun@soton.ac.uk

**Christina Vanderwel**

Aerodynamics and Flight Mechanics  
University of Southampton  
Southampton SO17 1BJ, UK  
c.vanderwel@soton.ac.uk

**Bharathram Ganapathisubramani**

Aerodynamics and Flight Mechanics  
University of Southampton  
Southampton SO17 1BJ, UK  
g.bharath@soton.ac.uk

### FRAMEWORK

Secondary flows in wall-turbulence remain a subject of active research despite the numerous investigations available in the literature. Their encounter has been reported in flows over a wide range of geometries which earned researchers curiosity such as surface conditions in curved surfaces ((Stroh *et al.*, 2016) to turbine blades ((Barros & Christensen, 2014)), as well as airfoil ribs surfaces ((?)). These secondary flows were shown to develop over heterogeneous surfaces whose all exhibit spanwise characteristic length scales which are comparable to the dominant length scale of flow, resulting in the so-called high- and low-momentum pathways (HMPs & LMPs) (Vanderwel & Ganapathisubramani, 2015; Anderson *et al.*, 2015). These surface perturbations were shown to lead to large modifications in the mean flow and turbulent stresses ((Mejia-Alvarez & Christensen, 2013)). While the mean and turbulent flow universality of such flows was examined previously ((Medjnoun *et al.*, 2018)) showing the inadequacy of the classical scaling laws to predict these flows, the development of these secondary flows past a heterogeneous to homogeneous step-change remains unexplored.

This experimental study aims to shed some light on this question by looking at the spatial evolution of these large-scale features along with their impact on the wall-drag and their interaction with the growing internal layer caused by the step-change.

### EXPERIMENTAL METHODOLOGY

#### Facility and surface heterogeneity

The experimental study was performed in an open-circuit suction wind tunnel at the University of Southampton (see Medjnoun *et al.* (2018) for more details).

The surface heterogeneity was modelled using two different smooth ridge profiles (e.i. rectangular and triangular shapes), made of clear perspex. Their nominal heights and spanwise spacings were 6 mm and 80 mm, chosen

to match 0.1 and 1 times the spanwise-averaged boundary layer thickness, respectively, in order to maximize potential secondary flows. Details about the geometrical characteristics of the heterogeneous surfaces are summarized in the table 1 below.

#### Oil-film interferometry

The wall shear-stress was directly measured through the interferometry technique. Dow Corning 200 Silicone oil droplets are deposited at various locations along the spanwise direction to assess the spanwise variation of the skin-friction. Their width is less than  $0.1\delta$  such that they are representative of independent skin-friction measurements. Interferograms are obtained by illuminating the droplets using a sodium lamp with a wavelength of 589 nm. A high-resolution LaVision Imager LX 16 MPixel CCD camera with a Nikon 200 mm AF Micro lens set at angle of  $25^\circ$  from the vertical were fitted to a Scheimpflug adapter to obtain respectively a large field of view and to satisfy the Scheimpflug condition (see figure 1). A single plane calibration target positioned at the wall in the  $(x, z)$ -plane was used to determine the mapping function through a third-order polynomial fit. This resulted in a FOV of approximately  $0.6S \times 1.2S$  in the  $(x, z)$ -plane (see figure 2). This allowed a simultaneous capture of the development of different spanwise interferograms. A series of 100 images per surface at a nominal speed of  $U_\infty = 20$  m/s are acquired for approximately 10 minutes in each run using LaVision DAVIS 8.2. This process was repeated several times at various streamwise locations such that to cover the variation of the skin-friction in the non-equilibrium region, and reconstruct a map of the skin-friction with the extent of  $8S \times 1.2S$  in the  $(x, z)$ -plane.

#### Planar and Stereo PIV

The boundary layer is diagnosed in both the streamwise-wall-normal plane  $(x, y)$  and the cross-plane

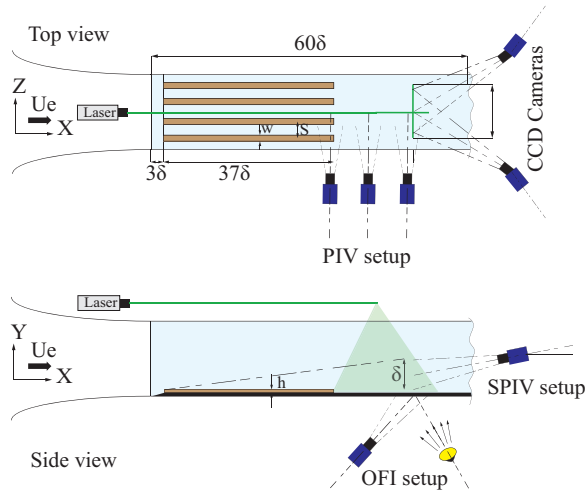


Figure 1. Schematics of the experimental arrangement of the surface step-change including the Planar/Stereo PIV setup (top) and the Oil-film interferometry setups (bottom).

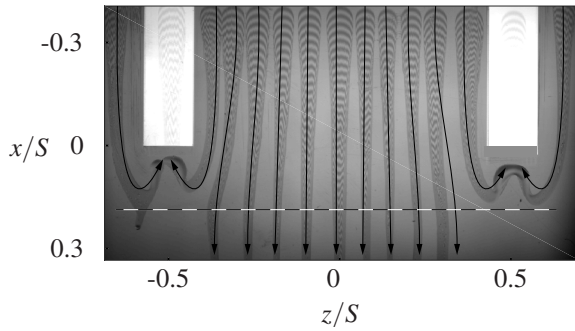


Figure 2. Example of de-warped interferograms at 20 m/s for the rectangular geometry case with drawn streamline following the pattern displayed by the OFI streaks.

$(y, z)$  using planar (2D2C) and stereoscopic (2D3C) PIV measurements respectively. While two spanwise locations were chosen at  $z/S = 0, 0.5$  for the planar, four different streamwise stations were performed for the SPIV. The flow is traced by vaporised glycerol-water solution particles generated by a Magnum 1200 fog machine, then illuminated with a laser light sheet sourced by a two-pulse Litron Nd:YAG laser operating at 250 mJ. A LaVision optical system for the beam focus/expansion of the light sheet is used, obtaining a relatively constant thickness in the measurement plane ( $\approx 1$  mm thickness). The particle images are recorded by two high-resolution LaVision Imager LX 16 MPixel CCD cameras fitted with Nikon 105 and 200 mm AF Micro lenses for the 2D2C and 2D3C PIVs respectively, with the latter being mounted on Scheimpflug adapters to account for the oblique view angle ( $\pm 42^\circ$ ), and are placed at nearly 1 m from the object plane. A single and a double-sided dual plane calibration target aligned with the laser light sheet were used to determine the mapping function for each setup, using a third-order polynomial fit. This resulted in a FOV of approximately  $2\delta \times 10\delta$  in the  $(x, y)$ -plane for the planar and  $2\delta \times 3\delta$  in the  $(y, z)$ -plane for the stereoscopic PIV. Using LaVision's DaVis 8.3 software, 3000 statistically independent realizations of images pairs are acquired for each case at 0.6 Hz, with a time de-

lay between two pulses of 50 and 20  $\mu s$  for the 2D2C and 2D3C PIVs respectively, at a free-stream velocity  $U_\infty$  of 20 m/s. This resulted in an average displacement of 15 and 7 pixels/s, which roughly translated to 0.6 to 1.5% bias uncertainty in the measurements (given the sub-pixel uncertainty being around  $\pm 0.1$  pixels). The velocity vector fields were subsequently obtained by interrogating particle images using a decreasing multipass scheme starting from 48 pixels  $\times$  48 pixels to a final pass of 16 pixels  $\times$  16 pixels and 24 pixels  $\times$  24 pixels with 50% overlap, resulting in an effective vector spacing of 0.5 and 0.55 mm for the 2D2C and 2D3C PIVs respectively.

## PRELIMINARY RESULTS

Table 1. Results summary: Subscripts referring to the four different streamwise stations with  $x_1/\delta_1 = -0.7$ ,  $x_2/\delta_1 = 0.25$ ,  $x_3/\delta_1 = 4$  and  $x_4/\delta_1 = 8.5$ .

Case	$h/\delta_1$	$S/\delta_1$	$S/\delta_2$	$S/\delta_3$	$S/\delta_4$
Rectangle	0.09	1.28	1.40	1.35	1.33
Triangle	0.08	1.15	1.27	1.40	1.44

Figure 2 illustrates the response of the oil film interferograms to the surface shear stress caused by both the surface spanwise heterogeneity and the streamwise step change, depicting changes in both wall shear stress magnitude and direction. It especially shows the presence of a recirculating motion past the step which is dominated by a highly three dimensional motion. Additionally, the interferograms indicate the approximate location of the reattachment region for the separated flow which is nearly  $2.5h$ . Additionally, the mean flow is shown to be affected as presented in figure 3. Similarly to previous studies, strong spanwise heterogeneities in the mean flow can be distinguished. These are represented in the form of alternating HMPs and LMPs between valleys and peaks respectively upstream the step-change. Figure 3 also shows, despite the presence of a step-change, the mean flow (further away from the wall) remains relatively unaffected while developing downstream. Interestingly, the near wall flow seems to be more affected by the step-change as the heterogeneity is shown to grow weaker further downstream.

The aforementioned changes in the mean flow topology are further substantiated by the identification of secondary motions through the computation of the vorticity-signed swirling strength  $\lambda_{ci}$ . The results are shown in figure 4 and indicate large-scale secondary flows associated with the surface heterogeneity. Similarly to the previous studies, these secondary flows consist of a pair of counter-rotating vortices formed on the top of either sides of the elevated strips. Besides the large-scale secondary flows, a new pair of small localized but high magnitude counter-rotating vortices of opposed sign take place above the strip. This new pair seems to not feature downstream the step, as opposed to the large secondary motions which pertain further downstream. This observation can partially explain why the outer mean flow downstream still remains unchanged since these large-scale secondary motions seem to inherently be capa-

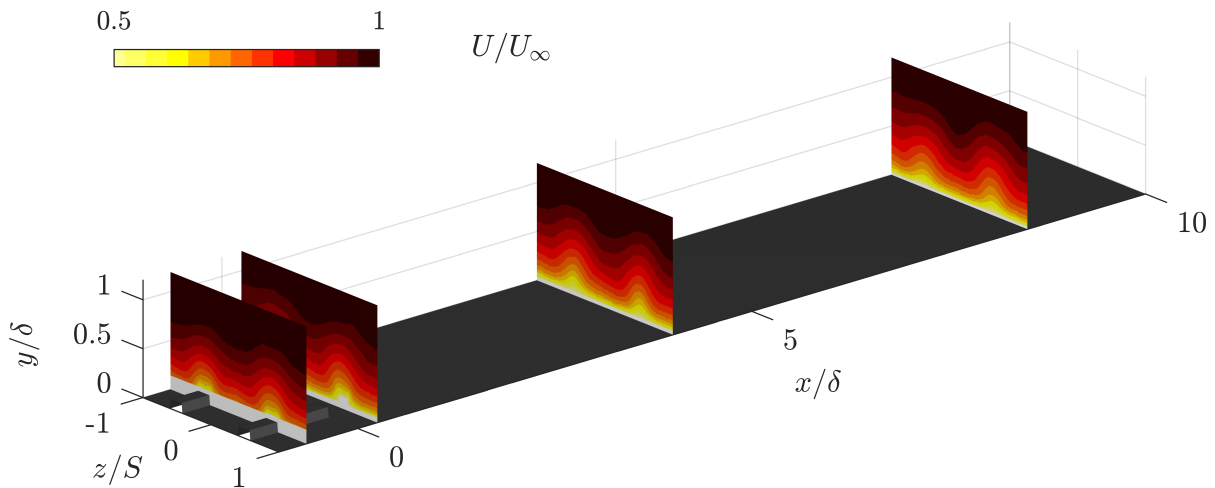


Figure 3. Cross-plane of the normalized mean streamwise velocity at the different streamwise locations for the rectangular case.

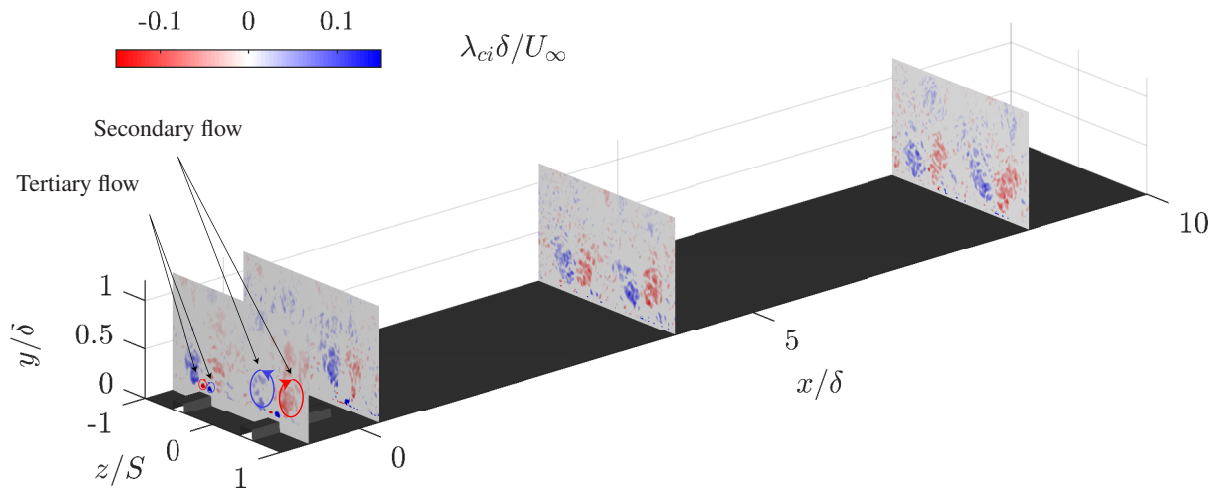


Figure 4. Cross-plane of the normalized mean vorticity-signed swirling strength at different streamwise locations for the rectangular case.

ble of sustaining their regenerationmselvesnger distances downstream of the step-cha and can maintain a good degree of similarity whilst flowing over the homogeneous ace. AtOn the contrary, thertiary flows seem to be incapable to self-sustain without a viscous boundary condition such an elevated strip, leading to the observed changes in the near wall.

#### FUTURE WORK

Further results and analysis addressing the above questions will be presented in greater detail in the final paper.

#### REFERENCES

Anderson, W., Barros, J. M., Christensen, K. T. & Awasthi, A. 2015 Numerical and experimental study of mechanisms responsible for turbulent secondary flows in boundary layer flows over spanwise heterogeneous roughness. *J. Fluid Mech* **768**, 316–347.

Barros, J. M. & Christensen, K. T. 2014 Observations of turbulent secondary flows in a rough-wall boundary layer. *J. Fluid Mech* **748**.  
 Medjnoun, T., Vanderwel, C. & Ganapathisubramani, B. 2018 Characteristics of turbulent boundary layers over smooth surfaces with spanwise heterogeneities. *J. Fluid Mech* **838**, 516543.  
 Mejia-Alvarez, R. & Christensen, K. T. 2013 Wall-parallel stereo particle-image velocimetry measurements in the roughness sublayer of turbulent flow overlying highly irregular roughness. *Phys. Fluids* **25** (11), 115109.  
 Stroh, A., Hasegawa, Y., Kriegseis, J. & Frohnappfel, B. 2016 Secondary vortices over surfaces with spanwise varying drag. *J. Turbul* **17** (12), 1142–1158.  
 Vanderwel, C. & Ganapathisubramani, B. 2015 Effects of spanwise spacing on large-scale secondary flows in rough-wall turbulent boundary layers. *J. Fluid Mech* **774**, R2.